http://dx.doi.org/10.14400/JDC.2014.12.2.439

치과 교정 물질에 따른 자기공명영상의 왜곡

송현옥[1,2], 임청환[1], 이상호[3], 양오남[1], 백창무[1], 정홍량[1]
한서대학교 보건의료학과[1], 익산병원 영상의학과[1], 서남대학교 방사선학과[3]

Distortion of Magnetic Resonance Imaging for Different Types of Orthodontic Material

Hyun-Og Song[1,2], Cheong-Hwan Lim[1], Sang-Ho Lee[3], Oh-Nam Yang[1], Chang-Moo Baek[1], Hong-Ryang Jung[1]
Dept. of Health Care, Hanseo University[1]
Dept.of Radiology, Ik-San Hospital[2]
Dept. of Radiological Science, Seonam University[3]

요 약 자기공명영상검사에서 치과 교정용 금속 물질에 의한 인공물(Artifact)의 영향을 평가하기 위해 치과 교정에 사용되는 와이어(Wire)와 브라켓(Bracket)을 재질별로 선택하여 비교 연구하였다. 치과 금속을 넣은 사각 아크릴 용기는 200 ×135 ×120 ㎜ 크기이며, 영상을 얻기 위하여 두부 코일을 사용하여 T_2강조영상, T1강조영상, FLAIR영상을 획득하였다. 획득된 시퀀스별 자기공명영상의 인공물을 평가하기 위하여 Image J 프로그램을 사용하여 인공물의 면적을 측정 비교하였다. 연구에서 치과 교정용 와이어와 브라켓의 인공물이 가장 큰 물질은 Stainless steel로 나타났다. 현재까지는 치과 교정에서 교정을 목적에 두고 금속 물질을 선택하였으나 치과 교정용 금속은 환자의 기능과 미의 특성뿐 아니라 자기공명영상 인공물 생성 여부도 함께 고려해야 한다. 추후 교정용 금속의 선택 및 개발 발전은 치아교정의 목적과 더불어 다른 분야도 고려해야 할 것으로 사료된다.

주제어 : 자기공명영상, 치과금속물질, 인공물, 치과교정용금속, 자기공명영상왜곡

Abstract To evaluate the effects of an artifact by metal material for orthodontics in Magnetic Resonance Image (MRI) examination, wires and brackets used in orthodontics were selected and compared. Using a head coil, a T_2-weighted image, T1-weighted image and FLAIR image were obtained. With obtained images, the sizes of the artifacts were measured and compared using Image J Program. In the research, the material with the biggest artifact in the wires and brackets for orthodontics was stainless steel wire. In the future, selecting and developing metal for correction should be considered also in other fields along with the purpose of orthodontics.

Key words : Metal artifact, Dental materials, Magnetic resonance image.

Received 2 January 2014, Revised 3 February 2014
Accepted 20 February 2014
Corresponding Author: Chung-Hwan Lim(Dept. of Health Care, Hanseo University)
Email: lch116@hanseo.ac.kr

ISSN: 1738-1916

1. Introduction

Cerebrovascular disease is common and a major cause of death. Each year, more than sixteen million new patients occur globally. The number of deaths caused by cerebrovascular diseases amounts to fifty three hundred thousand people. In Korea, the death rate of cerebrovascular diseases as of 2010 was 53.2 per one hundred thousand people, which accounted for the second highest cause of death following cancer. The occurrence of cerebrovascular diseases has continuously increased since 2000. In addition, the number of patients younger than forty years old has increased greatly.

As a society ages and medical technologies develop, biomedical metal materials are seen in many patients. These biomedical metal materials may be ineligible for MRI for safety reasons and due to artifacts. More attention should be paid to this as the intensity of the magnetic field of MR equipment increases.

Biomedical metal materials generate artifacts and bring about the loss of images. Metal materials in the oral cavity distort various images in MRI on the neck, the base of the brain, and the upper jaw. It is known that the distortions of MRI differ depending on the quality, shape, position, and direction of metal materials and the method of MRI examination. These artifacts make it difficult to make an accurate diagnosis. Thus, there have been continuous studies on efforts to reduce the artifacts, and continuous research is necessary in the future. Early diagnosis after the onset has great effects on the future treatment of cerebrovascular diseases. In particular, MRI for cerebrovascular diseases is a very important test for early detection and prevention. The quality of the magnetic resonance imaging is measured based on quantitative measurements of contrast, resolution, noise, image distortion, etc., or qualitatively compared with standard images. Among these, image distortions cause errors in anatomical diagnosis, resulting in errors in pathologic analysis or making images impossible to interpret. This calls for efforts for proper identification to remove the source of error and corresponding measures to maintain the best imaging quality.

With the trend of rising orthodontic practices by social influences and personal preferences, dental prostheses, orthodontic wires, brackets, implants, etc., have become sources of image distortion and diagnostic error. Therefore, there is a need for research into factors such as the selection of materials for dental metal materials and methods of inspection. It is known that metal materials such as gold crowns, dental titanium implants, metal orthodontic gear (wire, brackets, bands, etc.) cause distortions. Therefore, this study attempted to investigate the conditions of dental orthodontic fixtures required for MR tests under an assumption that the degree of artifacts could be minimized by dental orthodontic fixtures such as wires and brackets and their materials.

2. Subject and Method

Commercialized dental metal materials are made of various metal alloys, and these metals are composed of ferromagnetic materials, diamagnetic materials, paramagnetic materials, or mixtures of these materials in various ratios. Orthodontic metal materials can be categorized into wires and brackets, and dental metal materials commercialized for medical purposes have different shape, size, and compositions according to each method, purpose, and time. To evaluate the effects of dental orthodontic fixtures on artifacts in MRI, five types of dental wire and three types of dental brackets currently used in the course of treatment in dental clinics were selected (Table1).

This study investigated the image artifacts of the wires and brackets using an MRI device (Siemens 1.0T). The wires and brackets were put in a square plastic container filled with MRI phantom solution to

carry out an MRI examination. The square container used was an acrylic container with a 5-mm-thick cover (200 x 135 x 120 mm^3). The experiment was conducted with the wire at 35-mm height from the center.

〈Table 1〉 For visual inspection of the distortion components of dental materials

Dental materials	Composition with mass (%)
Nickel Titanium wire	Ti 50~70, Ni 30~50, Nb 10~20, Cu 5~10, Fe 1~5, Co 1~5
Titanium Molybdenum Wire	Ti 62~81.75, Zr 4.5~10, Sn 3.75~8, Mo 10~20
Nickel Cobalt Wire	Co 39.80, Cr 19.90, Ni 15.4, Fe 15.3, Mo 7.10, Mn 1.97, C 0.061, Si 0.478
Silver solder Wire	Ag 50~70, Cu 20~40, Zn 10~20, Sn 1~10
Stainless Steel Wire	Fe 69.5, Cr 18.0, Ni 9.0, Mn 2.0, Co 0.75
Ceramic Bracket	Alumina Oxide 99.9, Silicone Dioxide balance
Composite Bracket	Thermoplastic Polyurethane Medical Grade Diphenylmethane 4.4 Diinocyanate (MDI) Polyether Polyol based on Diropylenglygol
Stainless Steel Bracket	Fe 69.5, Cr 18.5, Ni 9.0, Mn 1.0, Co 0.75 Si, C, P, S : less than each 1% balance

Dental wires vary in size and type according to the degree and period of correction. Therefore, the commercialized wires used in the experiment were categorized into composing materials regardless of the maker and the size of the cross-sectional area variation. For the quantitative evaluation of dental wire distortion width in the MRI, the wires used were cut into 10-mm lengths.

In consideration of the effects of dental metal materials on the head and neck during an MRI, using a head coil, 3 different types of sequence imaging were obtained: T_2 weighted imaging (TR 4,990msec, TE 115 msec, flip angle 150°, FOV 190㎜, matrix size 202×256), T_1 weighted imaging (TR 443 msec, TE 14 msec, flip angle 90°, FOV 190㎜, matrix size 202×256), Flair (TR 7,900 msec, TE 109 msec, flip angle 150°, FOV 190㎜, matrix size 202×256) (Table 2).

〈Table 2〉 Distortion of magnetic resonance imaging for image parameters

Se \ P	TR (㎳)	TE (㎳)	f/a(°)	FOV (㎜)	matrix size
T2WI	4,990	115	150	190	202×256
T1WI	443	14	90	190	202×256
Flair	7,900	109	150	190	202×256

P : Parameter, Se : Sequence, f/a : flip angle

For evaluation of the images, Image J, a digital image analysis program, was used. Standard images were obtained without dental metal material, which were compared to images with a dental metal material, and the sizes of each distortion were measured.

3. Result

3.1 Evaluation of the MRI Without Dental Metals

Using MRI equipment, an image of the experimental container without wires or brackets was obtained, and the area of the image was measured using the Image J program. The overall area on the image obtained without dental metal alloys was 27,360.15㎟, and the area covered by the container in each imaging technique is as follows: FLAIR imaging 8,210.81㎟, T_1weighted imaging 8,203.17㎟, T_2 weighted imaging 8,203.65㎟ (Figure 1).

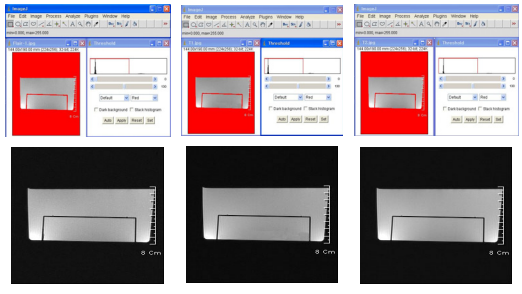

(a) (b) (c)

[Fig. 1] Without dental material magnetic resonance imaging and Image J image
(a) FLAIR Image (b) T_1 Image
(c) T_2 Image

3.2 Evaluation of the MRI with Dental Metals

3.2.1 Evaluation of image containing Ni-Ti wire

In the cross-sectional images of Ni-Ti wire in each sequence, the wire form was maintained under the view of the naked eye, and the cross-sectional areas of the wire in the total field of view were as follows: FLAIR imaging 0.018%, T_1 weighted imaging 0.019%, T_2 weighted imaging 0.018%. Distortions were not found in the sequential images.

When analyzing the sequential images in Image J, the areas including the wire were as follows: FLAIR imaging 4.88㎟, T_1 weighted imaging 5.20㎟, T_2 weighted imaging 5.02㎟. The areas measured in the images were expanded by 17.83x for FLAIR imaging, 18.97x for T_1 weighted imaging, and 18.33x for T_2 weighted imaging, compared to the actually measured cross-sectional area of 0.28㎟ (Table 3).

3.2.2 Evaluation of image containing Ti-Mo wire

In the cross-sectional images of Ti-Mo wire in each sequence, the wire form was maintained under the view of the naked eye, and the cross-sectional areas of the wire in the total field of view were as follows: FLAIR imaging 0.035%, T_1 weighted imaging 0.040%, T_2 weighted imaging 0.036%. Distortions were not found in the sequential images.

When analyzing the sequential images in Image J, the areas including the wire were as follows: FLAIR imaging 9.80㎟, T_1 weighted imaging 11.10㎟, T_2 weighted imaging 10.06㎟. The areas measured in the images were expanded by 49.62x for FLAIR imaging, 56.19x for T_1 weighted imaging, and 50.94x for T_2 weighted imaging, compared to the actually measured cross-sectional area of 0.20㎟ (Table 3).

3.2.3 Evaluation of image containing Ni-Co wire

In the cross-sectional images of Ni-Co wire in each sequence, the wire form was maintained under the view of the naked eye, and the cross-sectional areas of the wire in the total field of view were as follows: FLAIR imaging 0.56%, T_1 weighted imaging 0.60%, T_2 weighted imaging 0.56% and distortions were found in the sequential images.

When analyzing the sequential images in Image J, the areas including the wire were as follows: FLAIR imaging 153.63㎟, T_1 weighted imaging 165.08㎟, T_2 weighted imaging 154.29㎟. The areas measured in the images were expanded by 291.06x for FLAIR imaging, 312.76x for T_1 weighted imaging, and 292.31x for T_2 weighted imaging, compared to the actually measured cross-sectional area of 0.53㎟ (Table 3).

3.2.4 Evaluation of image containing silver solder wire

In the cross-sectional images of silver solderwire in each sequence, the wire form was maintained under the view of the naked eye, and the cross-sectional areas of the wire in the total field of view were as follows: FLAIR imaging 0.45%, T_1 weighted imaging 0.46%, T_2 weighted imaging 0.45%. Distortions were not found in the sequential images.

When analyzing the sequential images in Image J, the areas including the wire were as follows: FLAIR imaging 125.00㎟, T_1 weighted imaging 126.91㎟, T_2 weighted imaging 125.05㎟. The areas measured in the images were expanded by 96.05x for FLAIR imaging, 97.51x for T_1 weighted imaging, and 96.08x for T_2 weighted imaging, compared to the actually measured cross-sectional area of 1.30㎟ (Table 3).

3.2.5 Evaluation of image containing stainless steel wire

In the cross-sectional images of stainless steel wire in each sequence, the wire form was severely distorted under the view of the naked eye, and the cross-sectional areas of the wire in the total field of view were as follows: FLAIR imaging 3.18%, T_1 weighted imaging 3.70%, T_2 weighted imaging 3.34%.

Severe distortions were found in the sequential images.

When analyzing the sequential images in Image J, the areas including the wire were as follows: FLAIR imaging 872.65㎟, T_1 weighted imaging 1013.88㎟, T_2 weighted imaging 914.16㎟. The areas measured in the images were expanded by 5191.30x for FLAIR imaging, 6031.45x for T_1 weighted imaging, and 5438.23x for T_2 weighted imaging, compared to the actually measured cross-sectional area of 0.17㎟ (Table 3).

3.2.6 Evaluation of image containing ceramic bracket

In the cross-sectional images of the ceramic bracket in each sequence, the wire form was maintained under the view of the naked eye, and the cross-sectional areas of the wire in the total field of view were as follows: FLAIR imaging 0.77%, T_1 weighted imaging 0.81%, T_2 weighted imaging 0.79%. Distortions were not found in the sequential images.

When analyzing the sequential images in Image J, the areas including the wire were as follows: FLAIR imaging 211.36㎟, T_1 weighted imaging 223.77㎟, T_2 weighted imaging 217.09㎟. The areas measured in the images were expanded by 17.17x for FLAIR imaging, 18.17x for T_1 weighted imaging, and 17.63x for T_2 weighted imaging, compared to the actually measured cross-sectional area of 12.31㎟ (Table 3).

3.2.7 Evaluation of image containing composite bracket

In the cross-sectional images of the composite bracket in each sequence, the wire form was maintained under the view of the naked eye, and the cross-sectional areas of the wire in the total field of view were as follows: FLAIR imaging 0.49%, T_1 weighted imaging 0.52%, T_2 weighted imaging 0.49%. Distortions were not found in the sequential images.

When analyzing the sequential images in Image J, the areas including the wire were as follows: FLAIR imaging 134.54㎟, T_1 weighted imaging 142.30㎟, T_2 weighted imaging 135.07㎟. The areas measured in the images were expanded by 14.05x for FLAIR imaging, 14.86x for T_1 weighted imaging, and 14.11x for T_2 weighted imaging, compared to the actually measured cross-sectional area of 9.57㎟ (Table 3).

3.2.8 Evaluation of image containing stainless steel bracket

In the cross-sectional images of the stainless steel bracket in each sequence, the wire form was severely distorted under the view of the naked eye, and the cross-sectional areas of the wire in the total field of view were as follows: FLAIR imaging 7.11%, T_1 weighted imaging 9.20%, T_2 weighted imaging 7.99%. Severe distortions were found in the sequential images.

When analyzing the sequential images in Image J, the areas including the wire were as follows: FLAIR imaging 1947.13㎟, T_1 weighted imaging 2517.30㎟, T_2 weighted imaging 2187.60㎟. The areas measured in the images were expanded by 221.54x for FLAIR imaging, 286.41x for T_1 weighted imaging, and 248.90x for T_2 weighted imaging, compared to the actually measured cross-sectional area of 8.79㎟ (Table 3).

〈Table 3〉 Metal artifact of analysis using Image J

Sequ. / Metal(㎜)	Flair	T_1WI	T_2WI	Flair	T_1WI	T_2WI
	Measured area(㎟)			Artifact / Metal (rate)		
Ni-Ti W. (0.43×0.63)	4.88	5.20	5.02	17.83	18.97	18.33
Ti-Mo W. (0.45×0.45)	9.80	11.10	10.06	49.62	56.19	50.94
Ni-Co W. (r : 0.41)	153.63	165.08	154.29	291.06	312.76	292.31
Silver Solder W. (r : 0.64)	125.00	126.91	125.05	96.05	97.51	96.08
Stainless S. W. (0.41×0.41)	872.65	1,013.88	914.16	5,191.30	6,031.45	5,438.23
Ceramic B. (3.92×3.14)	211.36	223.77	217.09	17.17	18.17	17.63

Composite B. (3.48×2.75)	134.54	142.30	135.07	14.05	14.86	14.11
Stainless S. B. (3.74×2.35)	1,947.13	2,517.30	2,187.60	221.54	286.41	248.90

Se : Sequence, W : Wire, S : Steel, B : Bracket

4. Discussion

Distortions in MRI represent pixels that cannot accurately express the inspected tissue's components, and the inaccurate pixels cause distortions in MRI, hindering diagnosis. Among the many causes of distortion in MRI, the distortion due to metal materials depends on the magnetic fields, material components, unevenness in magnetic susceptibility, amount of metals, shape, direction, and placement. Also, magnetic susceptibility is one of the physical properties of the material, and it can be defined as a ratio of magnetic response of the substance to the active magnetic field.

There are 3 types of substances according to magnetic susceptibility: diamagnetic, paramagnetic, and ferromagnetic. Diamagnetic substances lack free orbit electrons, and are led to the opposite direction to the magnetic field by a weak external magnetic field., diamagnetic substances have small non-magnetic susceptibility and are basically non-magnetic.

Paramagnetic substances have free orbit electrons, and in an external magnetic field, the leading magnetic field faces relatively the same direction of the external magnetic field. Paramagnetic substances possess a strong force in a magnetic field region, which causes high chances of MRI distortion. Paramagnetic substances include iron, cobalt, nickel, etc. Of the orthodontic materials used in this study, the stainless steel wire showed expanded artifact/metal ratios as follows: FLAIR Imaging 5,191.30x, T_1 weighted imaging 6,031.45x, and T_2 weighted imaging 5,438.23x. The stainless steel bracket showed expanded artifact/metal ratios as follows: FLAIR Imaging 221.54x, T_1 weighted imaging 286.41x, and T_2 weighted imaging 248.90x.

Most clips and implants inserted or fixed in the body are made of non-magnetic substances such as titanium for medical purposes, but when a patient undergoes MRI with these materials in their body, the drop-out of signals on the surface of the metal causes distortions in imaging. Dental implant prosthetics, orthodontic screws, and aneurysm clips are a few examples of titanium alloys that cause distortions in MRI. artifact/metal ratio of FLAIR Imaging was 17.83x, that of T_1 weighted imaging was 18.97x, and that of T_2 weighted imaging was 18.33x for imaging with Ni-Ti wire. The artifact/metal ratio of FLAIR Imaging was 49.62x, that of T_1 weighted imaging was 56.19x, and that of T_2 weighted imaging was 50.94x for imaging with Ti-Mo wire. Also, all tissues surrounding metal materials showed small and large distortions, and although there were differences in width, it was determined that the cause of distortion was drop-out.

It has been known that orthodontic devices made from stainless steel alloy cause the largest image distortions, and because these orthodontic devices are attached at many points by non-ferrous materials and cannot be moved, clinically, the biggest problems are difficulties in imaging analysis due to distortions. Although there has been new research for various new sequences and unsolved signal correction by scientists for the improvement of image resolution around these metal substances to overcome these problems with distortion [11], there has not been a quantitative report on the measurement of the size of distortions caused by metal materials in MRI. There are few paradoxical results reported in documents regarding metal distortion in Spin Echo sequence, although little research has reported that there were no distortions by metals in the SE sequence. In contrast, many scholars reported that titanium alloy showed large or medium-sized imaging distortions in the SE sequence. The common claim in these is that the echo time is

shortened, and the distortion of images also decreases, but in this study, the conditions in each sequence differed, so a comparison could not be done. Also, the two important causes of imaging distortion are susceptibility and electrical conductivity, but in this study, the results were shown without conductivity in consideration.

Although when the conditions such as strength of the magnetic field, sequence, amount of ferromagnetic material, and the geometrical factors are the same, the images can show distortions due to differences in parameters, and titanium is known not to cause distortions in low magnetic area images. For these reasons, and because of the strength of titanium, the material is used widely as a dental material. this study, it was also confirmed that titanium alloy showed less distortion compared to other metals, and of the 3 sequences, the Flair imaging showed the least distortion. Therefore, nickel titanium wire has the least distortion among the currently used materials in orthodontic wires, and for the brackets, composite brackets showed the least distortion. Therefore, when considering only distortion, the combination of nickel titanium wire and composite brackets is the most ideal.

5. Conclusions

Biomedical metal produces artifacts in MRI. These artifacts cause damage and risk by magnetism in regard to the information about images in most areas around the metal devices. The biggest reason for the artifacts is metal retainers in dental materials in MRI. In this study, the material with the greatest artifacts in the wires and brackets for orthodontics turned out to be stainless steel alloy. Yet, the most preferred material is stainless steel alloy for metals in orthodontics. The choice of metal alloy for dental clinics should consider impacts under a magnetic field as well as the patient's biological compatibility, functionality, and aesthetic characteristics.

Thus, for a metal alloy in orthodontics, a patient's biological compatibility, functionality, aesthetics, and minimum generation of artifacts in MRI should be considered. Radiologists and MRI examiners should be aware of the effects of orthodontic devices in MRI on the head and neck and their impacts on the images. Therefore, it is expected that the results of this study will be used for MRI examination and image diagnosis of patients who were treated with the wires and brackets for orthodontics.

REFERENCES

[1] Z. Starčuk, K. Bartušek, H. Hubálková et al, Evaluation of MR artifacts caused by metallic dental implants and classification of the dental materials in use, Measurement Science Review, Vol.6(2), Section 2, 2006

[2] Jana Starčuková, Zenon Starčuk Jr., Hana Hubálková et al, Magnetic susceptibility and electrical conductivity of metallic dental materials and their impact on MR imaging artifacts, Dental Materials , Vol. 24, p715-723, 2008

[3] Marques JP, Bowtell R et al, Evaluation of a fourie based method for calculating susceptibility induced magnetic field perturbations, Proc Intl Soc Magn Reson Med, Vol. 11, p1020, 2003

[4] Andre LF. Costa, Simone Appenzeller, Clarissa-Lin Yasuda et al, Artifacts in brain magnetic resonance imaging due to metallic dental objects, Med Oral Patol Oral Cir Bucal, Vol. 14, p278-282, 2009

[5] Brown MA, Semelka RC et al, MRI : basic principles and applications. 2nd ed. New York: Wiley-Liss, 1995

[6] Shellock FG, Kanal E et al, Aneurysm clips : evaluation of MR imaging artifacts at 1.5T, Radiology, Vol. 209, p563-566, 1998

[7] Hashemi RH, Bradley WG. Jr et al, MRI : the basics. 1st ed. Baltimore: Williams & Wilkins.

[8] Bennett LH, Wang PS, Donahue MJ et al(1996), Artifacts in magnetic resonance imaging from metals, Journal of Applied Physics, Vol.79, p4712-4714, 1997

[10] Lissac M, Metrop D, Brugirard J et al. Dental Materials and Magnetic Resonance Image . Investifative Radiology Vol. 26, p40-45, 1991

[11] Rudisch A, Kremser C, Peer S et al, Metallic artifacts in magnetic resonance imaging of patient with spinal fusion. A comparison of implant materials and imaging sequence, Spine, Vol. 23, p692-699, 1998

[12] Teitelbaum GP, Bradley WG. Jr, Klein BD et al, MR imaging artifacts, ferromagnetism, and magnetic torque of intravascular filters, stents, and coils, Radiology, Vol. 166, p657-664, 1994

[13] Malik AS, Boyko O, Aktar N et al, A comparative study of MR imaging profile of titanium pedicle screws, Acta Radiol, Vol. 42, p291-293, 2001

[14] Ganapathi M, Joseph G, Savage R et al, MRI susceptibility artifacts related to scaphoid screws : the effect of screw thpe, screw orientation and imaging parameters, J Hand Surg, Vol. 27, p165-170, 2002

송 현 옥(Song, Hyun Og)

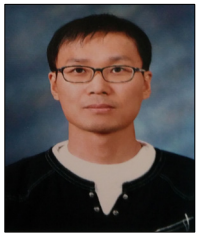

- 2013년 2월 : 한서대학교 대학원 방사선학과(방사선학석사)
- 2001년 2월 ~ 현재 : 익산병원 영상의학과 방사선사
- 관심분야 : 방사선학, 자기공명영상
- E-Mail : rad7579@daum.net

임 청 환(Lim Chung-hwan)

- 1997년 8월 : 단국대학교 보건행정학과(보건학 석사)
- 2005년 2월 : 경원대학교 의료경영학과(보건학 박사)
- 2001년 3월 ~ 현재 : 한서대학교 방사선학과, 보건의료학과 교수
- 관심분야 : 방사선학, 자기공명영상
- E-Mail : LCH116@hanseo.ac.kr

이 상 호(Lee. Sang Ho)

- 2009년 8월 : 한서대학교 방사선학과(방사선학석사)
- 2012년 3월 : 원광대학교 화학과 (이학박사)
- 2010년 8월 ~ 현재 : 서남대학교 방사선학과 교수
- 관심분야 : 방사선학, 분자영상
- E-Mail : ho8350@hanmail.net

양 오 남(Yang Oh Nam)

- 2013년 2월 : 한서대학교 방사선학과(방사선학석사)
- 2013년 3월 ~ 현재 : 한서대학교 보건의료학과 박사과정 재학
- 2013년 9월 ~ 현재 : 목포과학대학교 방사선과 교수
- 관심분야 : 방사선치료학, 보건학
- E-Mail : lando2000@daum.net

백 창 무(Baek Chang Moo)

- 1999년 2월 : 외국어대학교(문학사)
- 2012년 2월 : 한서대학교 방사선학과(방사선학석사)
- 2013년 3월 ~ 현재 : 한서대학교 보건의료학과 박사과정 재학
- 관심분야 : 방사선학, 보건학
- E-Mail : krea8or@gmail.com

정 홍 량(Jung. Hong Ryang)

- 1995년 2월 : 단국대학교 행정대학원 보건행정학과(보건학석사)
- 2004년 8월 : 순천향대학교 환경보건학과(보건학박사)
- 1999년 3월 ~ 현재 : 한서대학교 방사선학과 교수
- 관심분야 : 방사선학, 보건역학
- E-Mail : rjung@hanseo.ac.kr